Rotationally inelastic collisions of LiH with He: Quasiclassical dynamics of atom-rigid rotor trajectories[a)]

Aristophanes Metropoulos
Theoretical Chemistry Institute, National Hellenic Research Foundation, Athens 501/1, Greece
David M. Silver
Applied Physics Laboratory, The Johns Hopkins University, Laurel, Maryland 20707

(Received 4 April 1984; accepted 2 May 1984)

Rotationally inelastic cross sections for the LiH–He collision system are computed classically using a previously derived *ab initio* potential energy surface [D. M. Silver, J. Chem. Phys. **72**, 6445 (1980)]. The LiH is in its ground vibronic state and is initially taken to be in its $j = 1$ rotational state. The He is in its ground electronic state. The system is treated as an atom-rigid rotor interaction. The results are compared with previously computed cross sections derived from the same *ab initio* potential energy surface using the coupled states approximation for quantum mechanical scattering [E. F. Jendrek and M. H. Alexander, J. Chem. Phys. **72**, 6452 (1980)]. The theoretical total cross sections are averaged over a temperature distribution and are then compared with experimental measurements of corresponding cross sections for a rotationally resolved LiH beam ($j = 1$) incident on a He gas target in thermal equilibrium at room temperature [P. J. Dagdigian and B. E. Wilcomb, J. Chem. Phys. **72**, 6462 (1980)]. The agreement between classical, quantum and experimental results is discussed.

I. INTRODUCTION

This paper is part of a collaborative effort to investigate rotationally inelastic collisions between LiH and a He atom. In a previous publication[1] (paper I), an *ab initio* potential energy surface was determined using the diagrammatic many body perturbation theory through third order in the correlation energy. Both He and LiH were assumed to be in their ground electronic and vibronic states, respectively. The LiH was treated as a rigid rotor with bond length equal to the equilibrium distance of the ground vibronic state of the LiH molecule. The calculated *ab initio* points on the LiH–He interaction potential were fit to an analytic form. The overall accuracy of the final interaction potential is assumed to be within ~ 1 mhartree. In a second publication[2] (paper II), integral cross sections for rotational energy transfer in LiH (in its ground vibronic state) due to collision with He (in its ground electronic state) were obtained using several quantum mechanical procedures and two potential energy surfaces. For the present purposes, the relevant aspect of that work involved the use of the quantum mechanical coupled states approximation and the interaction potential described in paper I. The relative kinetic energy distribution was taken to be a combination of the Maxwell distribution of the He target gas and the monoenergetic distribution (nearly a δ function) of the LiH incident beam (see below). Three relative kinetic energies from the combined distribution were judiciously selected so as to imitate the results of a random sampling of the combined distribution with reasonable accuracy. Computations were carried out for three initial rotational states of LiH ($j = 0,1,2$) at each of these energies. The energy values of the combined distributions were assumed to be low enough so that only the rotational states of LiH could be excited during the collision. A third publication[3] (paper III) presented experimentally determined state resolved cross sections for the rotationally inelastic scattering of a nearly monoenergetic supersonic beam of LiH impinging on a He target gas at room temperature having a Maxwell distribution in the kinetic energy. The bulk of He and LiH were in their ground electronic and vibronic states, respectively. The LiH in the beam was rotationally state resolved at $j = 1$ by directing the beam through a quadrupole electric field before its incidence on the He gas. The experimental and quantal cross sections are in reasonable agreement.[3]

In the present work the quasiclassical trajectory method is applied to the LiH–He system in an effort to examine the validity of the classical approach vis-a-vis the experimental and accurate (coupled states) quantal results. Since in both the quantal and the classical computations the same accurate *ab initio* potential is employed, the advantages and limitations of the classical approach *per se* as well as the contributions of the quantum effects can be evaluated.

II. CLASSICAL MECHANICAL APPROACH

A. Formulation of the problem

The state to state cross sections for the system

$$\mathrm{LiH}(j = 1) + \mathrm{He} \rightarrow \mathrm{LiH}(j') + \mathrm{He}$$

are computed classically by integrating the canonical equations of motion over the potential energy surface obtained in paper I. An energy contour diagram of the surface appears in Fig. 1 and a projected view is provided in Fig. 2. The use of this surface is of course tantamount to fixing the vibronic and electronic states of the fragments to be the ground states. In particular, the LiH molecule is a rigid rotor with $R = R_e$ for the vibrational state $v = 0$ of the ground electronic state. The computations are carried out at the three energies used in paper II but only for the initial rotational state used in

[a)] This work was supported in part by the National Science Foundation under Grants CHE 76-11359 and CHE 78-08729, and in part by the Department of the Navy, Naval Sea Systems Command under Contract N00024-83-C-5301.

 0021-9606/84/161682-10$02.10

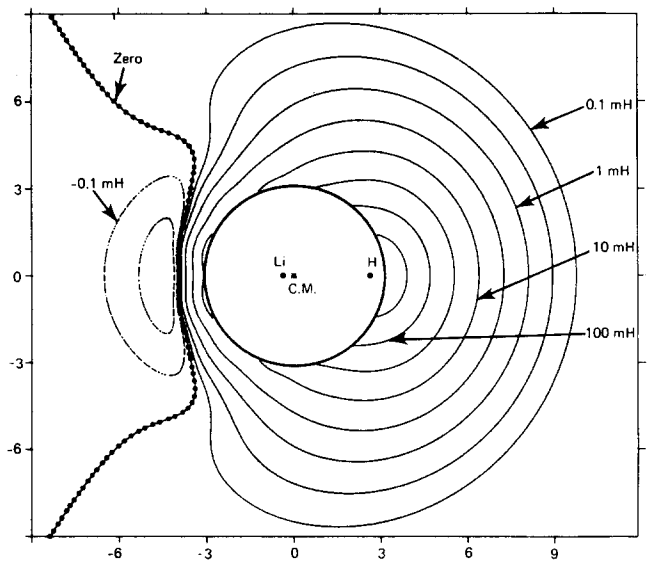

FIG. 1. Equipotential energy contour diagram of the analytic representation of the rigid rotor LiH–He interaction surface as a function of the distance (expressed in bohr) of the helium atom from the ^{7}LiH center of mass. Successive contours differ by a factor of $\sqrt{10}$ in energy (expressed in mhartree). The circle of radius 3 bohr, drawn around the ^{7}LiH center of mass, illustrates the anisotropy of the surface.

paper III, namely, $j = 1$. The cross sections for each "final state" and for each energy are obtained by binning the trajectories and are compared to the corresponding quantal cross sections given in paper II.

For a meaningful comparison with the experimental cross sections the collision energy of each trajectory must be drawn from a distribution similar to the experimental distribution; and enough trajectories must be generated to allow for a statistically valid comparison. However, it is expected that the cross sections computed on the basis of such a sampling would not be much different than the cross sections

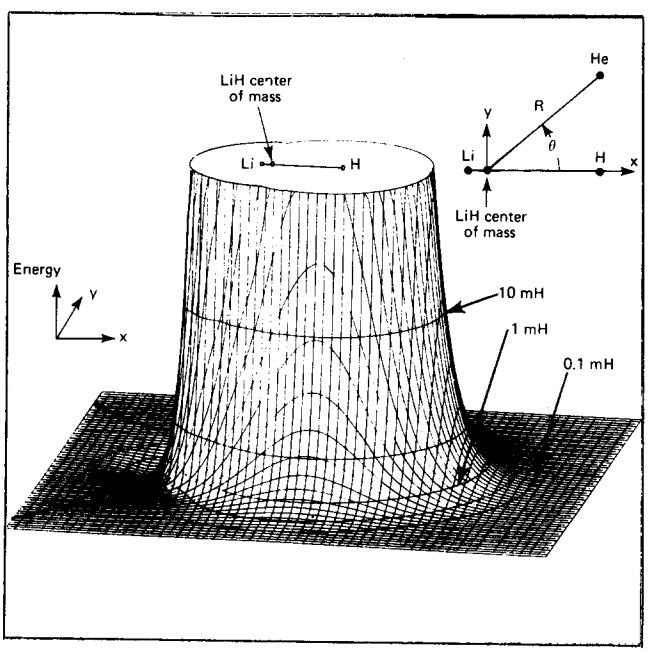

FIG. 2. Projected view of the LiH–He interaction surface truncated at the 0.5 eV energy contour level. The contour levels are the same as those in Fig. 1.

computed by using a few energies judiciously selected. This is the approach followed here and in paper II. One of the selected energies is the "average" of the relative energy distribution curve; the other two are selected equidistant from the average on either side of it. Then, the distribution weighted averages of the individual cross sections over these three energies yield the cross sections to be compared with the experimental cross sections obtained in paper III. We use the averaging method employed in paper II.

B. Cross section

The total energy of the LiH–He collision system is given by

$$E = E_k + V + E_R + \epsilon , \tag{1}$$

where E, E_k, V, E_R, and ϵ are the total, the relative kinetic, the interaction potential, the LiH rotational, and the LiH zero vibrational energies, respectively. For a given E (small enough to avoid any vibronic energy changes during collision), the rotationally inelastic cross section $\sigma_{j\to j'}(E)$ for the transition from the initial rotational state j to the final rotational state j' of LiH is given by

$$\sigma_{j\to j'}(E) = 2\pi \int_0^{b_{\max}} b \cdot P_{j\to j'}(b,E)\,db . \tag{2}$$

$P_{j\to j'}(b,E)$ is the transition probability as a function of E and of the impact parameter b; $b_{\max}$ is that b for which $P_{j\to j'}(b > b_{\max},E) = 0$ for all practical purposes.

In principle, if $P_{j\to j'}(b,E)$ were a known function of b, then Eq. (2) could be integrated by a standard Monte Carlo integration[4] with b as the variable of integration and $y = b \cdot P_{j\to j'}(b,E)$ as the integrand. Since the maximum value of y is $y_{\max} = b_{\max} \cdot [P_{j\to j'}(b,E)]_{\max} = b_{\max}$ and its minimum value is zero, the range of both b and y is $(0,b_{\max})$. Following the standard Monte Carlo integration procedure, a pair of random numbers (x_1,x_2) is drawn from a uniform distribution in the interval $(0,b_{\max})$, and the number $N_{j'}(E)$ of points lying on or below y, after a total of N draws, are counted. The dependence of $N_{j'}(E)$ on j' and E follows, of course, from the dependence of y on these parameters. Then, for large N (ideally ∞) the ratio $N_{j'}(E)/N$ is equal to the ratio of the area under the curve of y over the total area $y_{\max} \cdot b_{\max} = b_{\max}^2$ covered by the random pair (x_1,x_2). Since the area under the curve of y is equal to the integral in Eq. (2) the above procedure yields

$$\frac{\sigma_{j\to j'}(E)}{2\pi b_{\max}^2} = \lim_{N\to\infty}\left(\frac{N_{j'}(E)}{N}\right).$$

For sufficiently large N (depending on the desired accuracy) the above relation gives

$$\sigma_{j\to j'}(E) \approx 2\pi b_{\max}^2 [N_{j'}(E)/N] . \tag{3}$$

Now, since the functional dependence of $P_{j\to j'}(b,E)$ on b is not known *a priori*, $N_{j'}(E)$ is found by computing a number of trajectories N at one of the total energies E and counting the number of trajectories resulting in a j' final rotational state. Details on the trajectory computation are provided in the next section.

Since the above method assumes that $P_{j\to j'}(b,E)$ is continuous and yet it is obtained in discrete steps, quite a large

number N of trajectories must be computed to obtain reasonable accuracy. However, the amount of computation can be reduced drastically if Eq. (2) is expressed as the Riemann sum

$$\sigma_{j\to j'}(E) = 2\pi \sum_{i=1}^{n} b_i \cdot P_{j\to j'}(b_i,E) \cdot \Delta_{bi} ,$$

where the interval $(0,b_{\max})$ has been divided into n subintervals $\Delta b_i = b_{i+1} - b_i$. These subintervals need not be equal to each other. Nonetheless, if n is large enough they may be chosen so that $\Delta b_i = b_{\max}/n$. Pursuing this option we substitute Δb_i in the above equation to obtain

$$\sigma_{j\to j'}(E) = \frac{2\pi \cdot b_{\max}}{n} \sum_{i=1}^{n} b_i P_{j\to j'}(b_i,E) . \tag{4}$$

At this point there are two options one can choose from, depending on whether an accurate profile of $P_{j\to j'}(b,E)$ as a function of b is desired or not. If a profile is desired, a large enough number $N(b_i)$ of trajectories (depending on the required accuracy) is computed for each b_i at the selected total energy E and the number of trajectories $N_{j'}(b_i,E)$ resulting in a j' final rotational state is counted. Then, the transition probability at each b_i is taken to be

$$P_{j\to j'}(b_i,E) = N_{j'}(b_i,E)/N(b_i) .$$

Substituting this in Eq. (4) gives

$$\sigma_{j\to j'}(E) = \frac{2\pi \cdot b_{\max}}{n} \sum_{i=1}^{n} [b_i \cdot N_{j'}(b_i,E)/N(b_i)] .$$

The total number of trajectories required in this approach is $N = \Sigma_{i=1}^{n} N(b_i) \approx n \cdot N(b_i)$ and is still quite large if reasonable accuracy is expected. However, it has the added advantage over the method associated with Eq. (2) of providing an accurate profile of $P_{j\to j'}(b,E)$. On the other hand, if such a profile is not desired, one may assign one b_i in each subinterval and then compute a single trajectory with this b_i. Under these conditions, $P_{j\to j'}(b_i,E) = \delta_{j'j''(i)}$ for all b_i and E, and the number N of trajectories is equal to the number n of the subintervals of the Riemann sum. $j''(i)$ is a running index representing the final rotational state obtained with the trajectory associated with b_i. Upon substitution in Eq. (4) one obtains a running index representing the final rotational state obtained with the trajectory associated with b_i. Upon substitution in Eq. (4) one obtains

$$\sigma_{j\to j'}(E) = \frac{2\pi \cdot b_{\max}}{N} \sum_{i=1}^{N} b_i \delta_{j'j''(i)} , \tag{5}$$

where the E dependence enters indirectly via the proportion of trajectories resulting in a j' final state at each E. This method requires the least amount of computation for comparable accuracy with the previous two methods.[5–7] Since the trajectories are classical, a quantization scheme must be employed in conjunction with Eq. (5) in order to achieve cross sections for integer rotational states j'.

The velocity averaged cross sections are the weighted sums of the individual cross sections and they are given by the equation

$$\sigma_{j\to j'} = \sum_{k=1}^{3} g_k \cdot \sigma_{j\to j'}(E_k) , \tag{5'}$$

where the subscript k differentiates between the three total energies. The weights g_k are normalized (i.e., $\Sigma_{k=1}^{3} g_k = 1$) and they are functions of the He–LiH relative velocity, the LiH beam velocity, the temperature of the He gas, and the mass of the He atom. Their functional form is derived in paper II. Here, the relative velocities are obtained from the energies [see Eq. (6) in the following section], the beam velocity is $V_b \sim 4.6$ Å/dps (paper III), and the temperature of the He gas is $T = 298.3$ K.

C. Initial conditions

As stated in the previous section, in order to evaluate Eq. (5), a number of trajectories must be computed and the trajectories resulting in the desired final state must be counted. The computation of a trajectory is done by integrating the canonical equations of motion over the potential energy surface. The integration yields the final value of the angular momentum of LiH, and from the quantal relationship of $J'^2 = j'(j'+1)h^2$ the final rotational state j' is obtained by appropriate quantization (see the following sections).

There are certain initial conditions that must be set prior to carrying out each integration. These conditions depend on the coordinate system in use and they are tied to its orientation, which is essentially defined by them. La Budde and Bernstein[5] refer the position coordinates of all particles to a single Cartesian coordinate system; they introduce the rigidity of the rotor as a nonholonomic constraint via a Lagrange multiplier.[8] Here, however, we adopt the system of Chapman and Green.[6] The coordinates of relative motion (x, y, z) of the LiH–He system are referred to a Cartesian system centered at the center of mass of LiH. The coordinates of angular motion of LiH are the Euler angles θ,ϕ referred to the same Cartesian coordinate system. The interatomic distance r of LiH is held constant, thus introducing the rigidity of the rotor and eliminating one coordinate at the same time. In this system, the LiH is considered motionless while the He is moving relative to it. The coordinates of relative motion are identical to the coordinates of He and the LiH–He separation is $R = (x^2 + y^2 + z^2)^{1/2}$. The orientation of the Cartesian coordinate system is such that the He initially (meaning at the beginning of integration) moves in the yz plane with an initial velocity vector parallel to the z axis. The integration starts at a LiH–He separation R_0 large enough so that the potential is virtually zero for $R \geqslant R_0$. It is at such separations that the values of the canonical coordinates and the orientations of the momenta vectors may be known (initialized) with certainty since now the equations of motion depend only on the kinetic part of the Hamiltonian (see the following section). Since the potential never becomes zero, the value of R_0 is selected by a couple of trial runs, and it is a trade off between cost and accuracy. Here, $R_0 = 15$ Å has been selected for which $V < 10^{-20}$ ergs($\sim 10^{-10}$ hartree). The same R_0 is used for each trajectory since there is nothing to be gained by varying it. In keeping with the chosen orientation of the Cartesian coordinate system, the canonical coordinates of motion of He are initialized as follows:

$$x_0 = 0 , \quad y_0 = b , \quad z_0 = (R_0^2 - b^2)^{1/2} ,$$
$$P_{x_0} = 0 , \quad P_{y_0} = 0 , \quad P_{z_0} = -\mu \cdot v_0 ,$$

where b is chosen randomly (see below), μ is the LiH–He reduced mass, and v_0 is the initial velocity of He. v_0 is obtained from Eq. (1) by setting $V=0$ and $E_R = B_e \cdot j(j+1)\hbar^2$ with $B_e = 1/(2\mu' r_e^2)$ where r_e is the LiH equilibrium distance used in paper I, μ' is the LiH reduced mass, and $j=1$. Substituting these values in Eq. (1) gives

$$v_0 = [2(E-\epsilon-2B_e\hbar^2)/\mu]^{1/2}. \tag{6}$$

The canonical coordinates of LiH are initialized as follows:

$$P_{\phi_0} = j_z\hbar,$$

$$P_{\theta_0} = s[j(j+1)\hbar^2(\sin^2\theta_0 - \cos^2\eta_0)]^{1/2}/\sin\theta_0$$

$$= s\cdot 2^{1/2}\cdot\hbar\cdot(\sin^2\theta_0 - j_z^2/4)^{1/2}/\sin\theta_0,$$

where η_0 is the initial angle between the angular momentum vector and the z axis, j_z is the quantum number of the z projection of the angular momentum vector, $j=1$ so that $\cos\eta_0 = j_z\hbar/[j(j+1)]^{1/2}\hbar = j_z/(\sqrt{2})$, and s is the sign of P_{θ_0}. The initial values θ_0, ϕ_0 of the Euler angles as well as j_z, s, and b are selected by random sampling from a uniform distribution between appropriate limits. Note that the initialization of P_θ and P_ϕ is guided by quantal considerations (i.e., quasiclassical approach) as is the random initialization of j_z and θ described in the next paragraph.

In this paper, θ_0, ϕ_0 (the initial values of θ, ϕ), b, j_z, and s are considered random variables uniformly distributed within their respective ranges. This corresponds to the randomness of these variables in an experimental setup. In the case of the coordinates of He, this randomness enters the picture indirectly through the orientation of the LiH-centered Cartesian coordinate system relative to a space fixed coordinate system. For each trajectory, the LiH centered coordinate system is rotated relative to the space fixed coordinate system so as to keep constant the initial values of the He coordinates. Returning now to the initializations, the range of j_z is taken to be the subset of integers $(-1,0,1)$ in order to mimic the quantized nature of j_z. The range of s is the subset $(-1,1)$. The random sampling of j_z and s from their respective intervals is done here indirectly by subdividing the range of a uniform random number generator into three and two equal regions, respectively. Then a random number is drawn and, depending on which of the equal regions it belongs to, an integer is assigned to j_z and s from their respective ranges. The initialization of θ is tied to the initial value of j_z through the angle η_0. Since $\cos\eta_0 = j_z/\sqrt{2}$ (for $j=1$) and $j_z = -1,0,1$ it follows that $\eta_0 = \pi/2, \pi/4, 3\pi/4$, respectively. Since the angular momentum vector of LiH is perpendicular to its plane of rotation, it is obvious that if $\eta_0 = \pi/2$, the range of θ_0 is $(0,\pi)$ while if $\eta_0 = \pi/4, 3\pi/4$ the range of θ_0 is $(\pi/4, 3\pi/4)$. Accordingly, $\cos\theta_0$ is sampled from the interval $(-1,1)$ if $\eta_0 = \pi/2$, and from the interval $(-1/\sqrt{2}, 1/\sqrt{2})$ if $\eta_0 = \pi/4$ or $3\pi/4$. The reason for sampling $\cos\theta_0$ rather than θ_0 is the same as that given by other authors.[5–7] Finally ϕ and b are initialized by sampling their respective ranges, namely, $(0,2\pi)$ and $(0,b_{\max})$. All the above samplings are done by using a uniform random number generator.

D. Canonical equations of motion

The canonical equations of motion can be easily derived once the Hamiltonian of the system is known.[8] Such a set of equations is given by Chapman and Green.[6] These equations are reproduced here in order to establish the notation and to correct a typographical error[6] in the equation for $\dot{P}_\phi$. Let α be the angle between $\mathbf{r}$ and $\mathbf{R}$; $M_{\rm Li}$, $M_{\rm H}$, and $M_{\rm He}$ be the atomic masses of Li, H, and He, respectively; $C_{\rm amu}$ be the conversion constant between atomic mass units and the mini cgs mass units used here (see below and Table I); and let L_k and P_l be the Laguerre and Legendre polynomials, respectively. Then, the canonical equations of motion are given by the following relations:

$$\mu' = \frac{m_{\rm Li}\cdot m_{\rm H}}{(m_{\rm Li}+m_{\rm H})}\cdot C_{\rm amu},$$

$$\mu = \frac{(m_{\rm Li}+m_{\rm H})\cdot m_{\rm He}}{m_{\rm Li}+m_{\rm H}+m_{\rm He}}\cdot C_{\rm amu},$$

$$B_e = 1/(2\cdot\mu'\cdot r_e^2),$$

$$R^2 = x^2+y^2+z^2,$$

$$\cos\alpha = (x\cdot\sin\theta\cdot\cos\phi + y\cdot\sin\theta\cdot\sin\phi + z\cdot\cos\theta)/R,$$

$$V(R,\cos\alpha) = \sum_{l=0}^{l_{\max}}\sum_{k=1}^{2} A_{kl}\cdot L_k[\alpha_l(R-a)] \cdot\exp[-\alpha_l(R-a)/2]\cdot P_l(\cos\alpha), \tag{7}$$

$$H = \frac{1}{2\mu}(P_x^2+P_y^2+P_z^2) + B_e\left(P_\theta^2 + \frac{P_\phi^2}{\sin^2\theta}\right) + V(R,\cos\alpha), \tag{8}$$

$$\dot{x} = P_x/\mu, \quad \dot{y} = P_y/\mu, \quad \dot{z} = P_z/\mu, \tag{9a}$$

$$\dot{\theta} = 2\cdot B_e\cdot P_\theta, \quad \dot{\phi} = 2\cdot B_e\cdot P_\phi/\sin^2\theta, \tag{9b}$$

$$\dot{P}_x = -\frac{\partial v}{\partial R}\frac{x}{R} - \frac{\partial v}{\partial\cos\alpha}\left(\frac{\sin\theta\cdot\cos\phi}{R} - \frac{x\cdot\cos\alpha}{R^2}\right), \tag{9c}$$

$$\dot{P}_y = -\frac{\partial v}{\partial R}\frac{y}{R} - \frac{\partial v}{\partial\cos\alpha}\left(\frac{\sin\theta\cdot\sin\phi}{R} - \frac{y\cdot\cos\alpha}{R^2}\right), \tag{9d}$$

$$\dot{P}_z = -\frac{\partial v}{\partial R}\frac{z}{R} - \frac{\partial v}{\partial\cos\alpha}\left(\frac{\cos\alpha}{R} - \frac{z\cdot\cos\alpha}{R^2}\right), \tag{9e}$$

$$\dot{P}_\theta = \frac{2\cdot B_e\cdot P_\phi^2\cdot\cos\theta}{\sin^3\theta} - \frac{\partial v}{\partial\cos\alpha}[\cos\theta\cdot(x\cdot\cos\phi + y\cdot\sin\phi) - z\cdot\sin\theta]/R, \tag{9f}$$

$$\dot{P}_\phi = \frac{\partial v}{\partial\cos\alpha}[\sin\theta\cdot(x\cdot\sin\phi - y\cdot\cos\phi)]/R. \tag{9g}$$

TABLE I. Units and physical constants.

Units			Physical constants	
	Mini cgs	cgs	Symbol	Values
			ϵ	0.086 4 eV[a]
Mass	1 ppg	10^{-24} g	$\hbar$	1.054 592 cperg dps
			h	6.626 196 cperg dps
Length	1 Å	10^{-8} cm	$\sqrt{e}$	1.594 900 Å[b] (3.013 925 bohr)
Time	1 dps	10^{-13} s	$m_{\rm Li}$	7.016 amu[c]
Energy	1 cperg	10^{-14} ergs	$m_{\rm H}$	1.007 825 amu[c]
			$m_{\rm He}$	4.002 6 amu[c]

[a] 1 eV = 160.219 177 cpergs, 1 hartree = 4359.828 cpergs.
[b] 1 Å = 1.889 727 bohr.
[c] 1 amu = 1.660 531 ppg (^{12}C base).

The meanings of the various potential constants in Eq. (7) are fully discussed in Ref. 1. The evaluation of the derivatives $\partial v/\partial R$ and $\partial v/\partial \cos\alpha$ is straightforward and will not be shown here.

E. Computation of trajectories

The numerical integration of the canonical equations of motion [Eqs. (9)] is accomplished by using a Runge–Kutta–Gill integrator[9] with variable step. Each integration yields a particular trajectory with characteristics depending on the initial conditions selected for that trajectory. Each integration starts at R_0 and it is carried out to a post collision distance equal (or nearly equal) to R_0. Before the main body of the computations was executed, a few trajectories were run and the total energy E and the total angular momentum M were monitored throughout the trajectory to make sure they were conserved. The following equations were used for this purpose (J and L are the molecular and translational angular momenta, respectively):

$$J^2 = P_\theta^2 + P_\phi^2/\sin^2\theta\,,$$

$$E - \epsilon = (P_x^2 + P_y^2 + P_z^2)/2\mu + B_e \cdot J^2 + V(R,\cos\alpha)\,,$$

$$L_x = y \cdot P_z - z \cdot P_y\,,$$

$$L_y = z \cdot P_x - x \cdot P_z\,,$$

$$L_z = x \cdot P_y - y \cdot P_x\,,$$

$$L^2 = L_x^2 + L_y^2 + L_z^2\,,$$

$$\mathbf{M} = \mathbf{J} + \mathbf{L}\,,$$

$$M^2 = [L_x - P_\theta \cdot \sin\phi - P_\phi \cdot \cos\theta \cdot \cos\phi/\sin\theta]^2 + [L_y + P_\theta \cos\phi - P_\phi \cdot \cos\theta \cdot \sin\phi/\sin\theta]^2 + [L_z + P_\phi]^2\,.$$

The initial step size of the integrator and the requested accuracy were set so that $E - \epsilon$ and M were kept constant to ten significant digits in the mini cgs units shown in Table I. Also, these trial trajectories were back integrated to check the consistency of the algorithm.

After the internal accuracy parameters were set and the program was thoroughly checked for consistency and accuracy, three batches of about 1150 trajectories each were run. Each batch was run at one of the total energies used in paper II, namely, $E = 0.2921$, 0.3921, and 0.4921 eV. The trajectories at $E = 0.3921$ eV were run first, in small batches of 100–500 trajectories each until the computed cross section did not change appreciably with additional trajectories. The same number of trajectories that accomplished this at $E = 0.3921$ eV was then used at the other two energies. At each of these energies, the trajectories were run in two batches of about 500 trajectories. This was mainly a safety precaution to minimize costs in case of an error or a computer failure. As it turned out, the uniform random number generator we were using was somewhat biased and generated more numbers in some regions of its range than in others. To partially rectify this, enough additional trajectories, about 10% of the total number of trajectories, were run in the less populated regions to make the total interval $(0,b_{\max})$ as uniform as possible. The effect of this rectification on the final cross sections was negligible. Therefore, no such rectification for the other random variables was attempted. Note, however, that the distribution of j_z and s was not affected by the small bias of the generator, because of the way these variables were sampled. The exact number of trajectories including rectification was as follows: 1164 trajectories at $E = 0.2921$ eV, 1178 trajectories at $E = 0.3921$ eV, and 1141 trajectories at $E = 0.4921$ eV. All computations were performed in FORTRAN on the IBM-3033 MP computer of the JHU/APL computing center. An average of about 4 s computing time was required for each trajectory excluding all subsequent computations and data manipulation. This relatively long computing time is attributed to the modularity of our program and to the Runge–Kutta–Gill integrator, which may loop in a particular region of the trajectory, each time halving the step size until the desired accuracy is achieved. Up to twenty such iterations at a particular point, starting from the initial step size, are allowed, after which further computation of this trajectory is abandoned. About 1% of the trajectories were lost for this reason. No doubling of the initial step size was allowed even if the potential was smooth enough to permit it. However, fractional values of the initial step size were allowed to increase with each iteration up to the initial value, if the potential was smooth enough for the computations to be within the desired accuracy.

The system of units used here is shown in Table I and it is the same as that used by LaBudde and Bernstein.[5] The unit prefixes d, c, p stand for deci-, centi-, pico-, respectively; for instance, a dps (decipicosecond) is equivalent to $10^{-1} \cdot 10^{-12} = 10^{-13}$ s. Table I also shows the values of the physical constants used here as well as some energy related parameters. The accuracy of the numbers is not necessarily the one implied by the number of digits. Nonetheless, all of these digits were retained in our program. The values of the coefficients of the potential are given in I. The value of r_e used here and in I is taken from a paper by Pearson and Gordy.[10]

F. Quantization of final J

Each trajectory results in a particular final angular momentum of LiH. In order to obtain cross sections, these momenta must be quantized, i.e., rotational quantum numbers must be extracted for each of the classical rotational angular momenta. This is done here by solving the quantal relation $J^2 = j_c'(j_c' + 1) \cdot h^2$ for j_c', with J equal to the obtained classical angular momentum, and then quantizing j_c'. The quantization of j_c' is performed using two different binning algorithms, and two slightly different results are obtained.

Let j' represent the quantized j_c'. Then, according to the first algorithm, if $j_c' \leqslant 0.5$, then $j' = 0$, and the corresponding b is added to the sum in Eq. (5) for $j' = 0$; if $k - 0.5 < j_c' \leqslant k + 0.5$, then $j' = k$, and the corresponding b is added to the sum in Eq. (5) for $j' = k$. For lack of a better name, this method is called the direct binning method. According to the second algorithm, the sums in Eq. (5) for two consecutive j' are incremented by a proper fraction $Q_{j'}$ of b (the b associated with the trajectory resulting in j_c') in proportion to how close to each $j' = k - 1$, k $(k = 1,2,3,\ldots)$ j_c' is; where $(k - 1 \leqslant j_c' \leqslant k)$. Each $Q_{j'}$ is computed as follows:

$Q_{k-1} = 1 - (j_c' - [j_c'])$, $Q_k = j_c' - [j_c']$, where $[j_c']$ is the integer part of j_c'. Accordingly, $b \cdot Q_{k-1}$ and $b \cdot Q_k$ are added to the sums in Eq. (5) for $j' = k - 1$ and $j' = k$, respectively. For instance, if $j_c' = 2.3$ $(2 < j_c' < 3)$, it follows that $Q_2 = 0.7$, $Q_3 = 0.3$; then the sums in Eq. (5) for $j' = 2,3$ are incremented by $0.7b$ and $0.3b$, respectively. This method is called the proportional binning method. Notice that according to this algorithm a specific j' cannot be assigned to each trajectory. Equation (5) is now slightly modified in order to incorporate formally the above binning procedures, it becomes

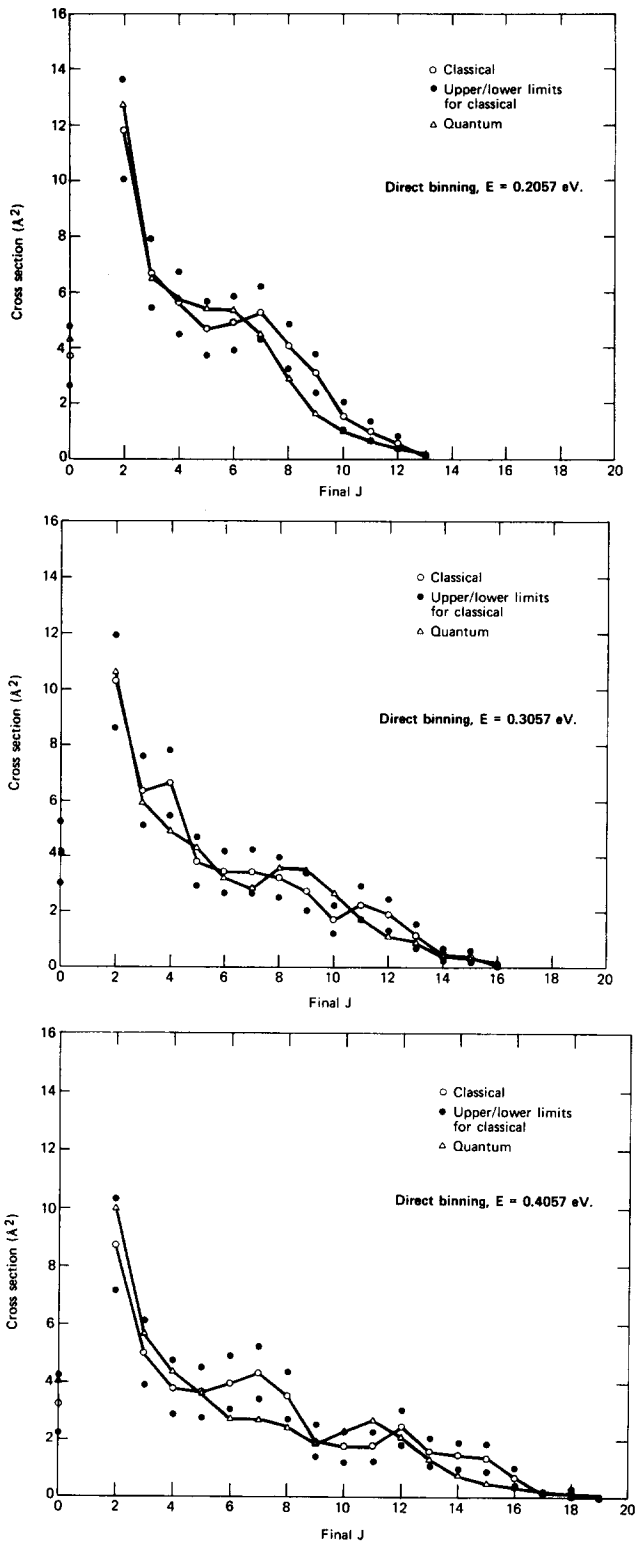

FIG. 3. Integral cross sections for rotational energy exchange as function of final rotational quantum number using the direct binning method. Error bounds on the classical results indicate 90% confidence limits. The relative kinetic energy is (A) 0.2057 eV, (B) 0.3057 eV, (C) 0.4057 eV.

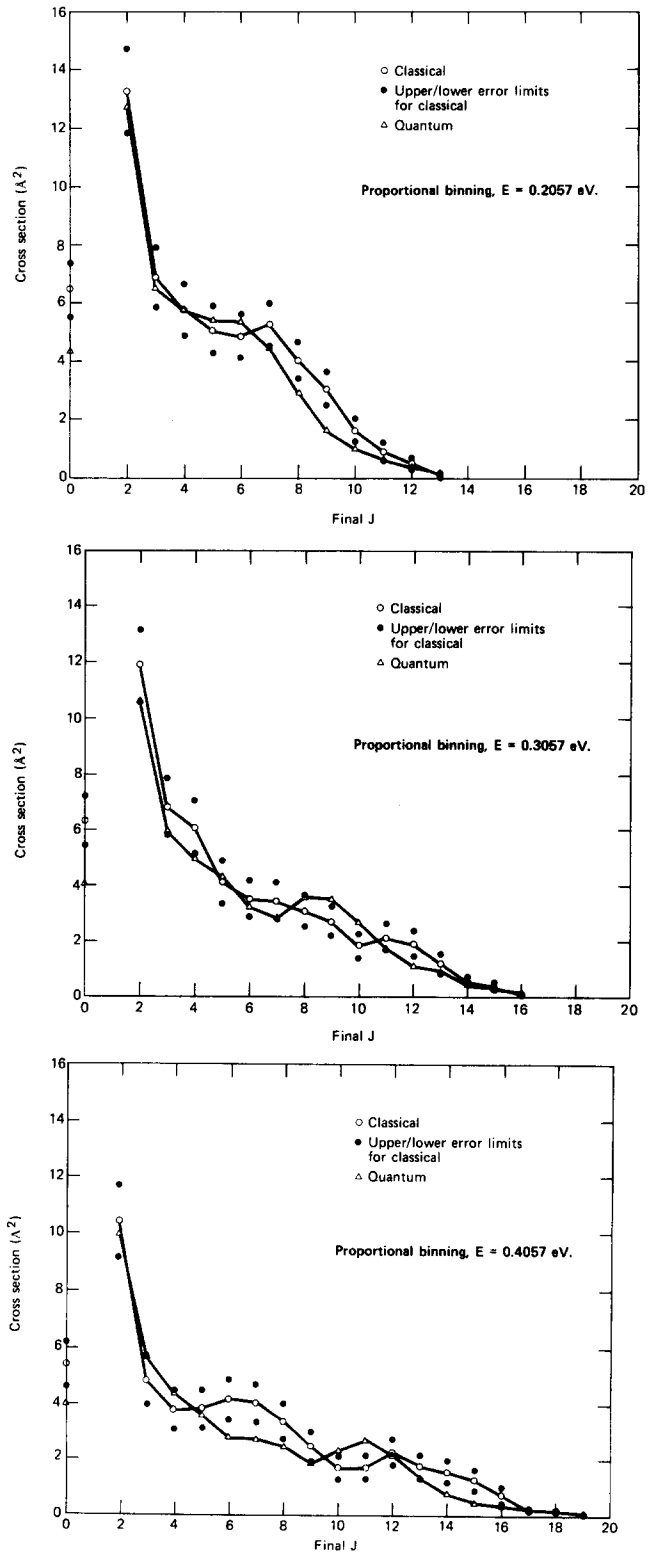

FIG. 4. Integral cross sections for rotational energy exchange as function of final rotational quantum number using the proportional binning method. Error bounds on the classical results indicate 90% confidence limits. The relative kinetic energy is (A) 0.2057 eV, (B) 0.3057 eV, (C) 0.4057 eV.

$$\sigma_{j\to j'}(E) = \frac{2\pi \cdot b_{\max}}{N} \sum_{i=1}^{N} b_i \cdot Q_{j'}(i)\delta_{j'j''}(i)$$

or

$$\sigma_{j\to j'}(E) = \frac{2\pi \cdot b_{\max}}{N} \sum_{i=1}^{N} b_{ij'} \cdot Q_{j'}(i), \quad (10)$$

where the subscript j' of b_i is a reminder that only b's of trajectories resulting in a j' final state are included in the sum. If the direct binning method is used, $Q_{j'} = 1$ for every j'. If the proportional binning method is used, $Q_{j'}$ is computed as above. Figures 3 and 4 show the resulting cross sections computed according to the direct and the proportional methods, respectively, as functions of j'; these results are also tabulated in Table II (the indicated error bounds are dealt with in the following section). For comparison, the corresponding quantal cross sections (from paper II) vs j' are also plotted in Figs. 3 and 4. Notice that the proportional binning method gives somewhat better cross sections (meaning smoother graphs) for all but $j' = 0$. This j' being the lower limit accumulates a disproportioned number of fractional b's.

The velocity averaged classical cross sections, obtained from the individual cross sections for each energy E (com-

TABLE II. Quantal and classical cross sections as functions of final J and total energy.

			Direct binning		Proportional binning	
Total energy (eV)	Final J	Quantum CS (Å^2)	Classical CS (Å^2)	Error (Å^2)	Classical CS (Å^2)	Error (Å^2)
0.2921	0	4.32	3.71	1.07	6.45	0.93
	1	49.30	43.28	3.47	38.43	2.91
	2	12.72	11.81	1.78	13.24	1.43
	3	6.49	6.67	1.27	6.89	1.03
	4	5.75	5.63	1.10	5.78	0.89
	5	5.41	4.68	0.96	5.08	0.81
	6	5.36	4.90	0.96	4.86	0.75
	7	4.47	5.26	0.94	5.28	0.75
	8	2.93	4.08	0.79	4.05	0.63
	9	1.60	3.11	0.70	3.04	0.56
	10	1.00	1.53	0.50	1.64	0.39
	11	0.64	0.99	0.37	0.92	0.30
	12	0.38	0.57	0.26	0.52	0.20
	13	0.19	0.10	0.11	0.12	0.10
0.3921	0	4.08	4.15	1.11	6.31	0.89
	1	45.50	43.33	3.43	39.42	2.93
	2	10.61	10.28	1.66	11.87	1.28
	3	5.96	6.35	1.23	6.81	1.00
	4	4.93	6.63	1.18	6.07	0.94
	5	4.31	3.80	0.89	4.12	0.74
	6	3.23	3.44	0.78	3.52	0.64
	7	2.83	3.44	0.80	3.45	0.63
	8	3.59	3.24	0.73	3.09	0.57
	9	3.51	2.74	0.66	2.71	0.54
	10	2.66	1.71	0.51	1.83	0.42
	11	1.75	2.27	0.60	2.13	0.47
	12	1.09	1.89	0.55	1.89	0.47
	13	0.92	1.13	0.43	1.19	0.37
	14	0.39	0.47	0.25	0.51	0.20
	15	0.30	0.41	0.23	0.35	0.18
	16	0.14	0.09	0.09	0.09	0.08
0.4921	0	4.05	3.25	0.99	5.42	0.80
	1	43.10	44.67	3.51	40.86	3.05
	2	9.99	8.72	1.58	10.42	1.27
	3	5.67	5.02	1.11	4.84	0.89
	4	4.37	3.82	0.92	3.78	0.71
	5	3.60	3.66	0.87	3.82	0.69
	6	2.76	3.98	0.91	4.17	0.73
	7	2.73	4.34	0.90	4.03	0.69
	8	2.45	3.55	0.82	3.36	0.63
	9	1.84	1.95	0.57	2.46	0.52
	10	2.32	1.77	0.54	1.68	0.40
	11	2.71	1.78	0.53	1.70	0.40
	12	2.11	2.46	0.62	2.24	0.48
	13	1.32	1.58	0.50	1.74	0.42
	14	0.74	1.46	0.46	1.53	0.38
	15	0.46	1.38	0.47	1.25	0.37
	16	0.33	0.70	0.33	0.73	0.29
	17	0.20	0.11	0.13	0.19	0.11
	18	0.14	0.16	0.14	0.14	0.11
	19	0.08	0.01	0.02	0.02	0.02

puted by both the direct and the proportional binning methods) are shown in Fig. 5 as functions of j'. The velocity averaged quantal cross sections (recomputed from paper II), as well as the experimental cross sections (from paper III), are also shown in Fig. 5 as functions of j'. The same results are tabulated in Table III.

G. Accuracy of the computations

For the purpose of estimating the errors introduced by the Monte Carlo calculations, the previously derived cross section equations are recast in a form more appropriate for error analysis. Let us define the following functions:

$$f(j',b,E) = 2\pi \cdot b \cdot P_{j\to j'}(b,E),$$
$$\phi(j',b_i,E) = 2\pi \cdot b_{\max} \cdot b_{ij'} \cdot Q_{j'}, \tag{11}$$

where $P_{j\to j'}(b,E)$ is taken to be the correct mathematical expression for the transition probability. Then, Eq. (2) may be recast in the following form:

$$csm_{j'} = \int_0^{b_{\max}} f(j',b,E)db,$$

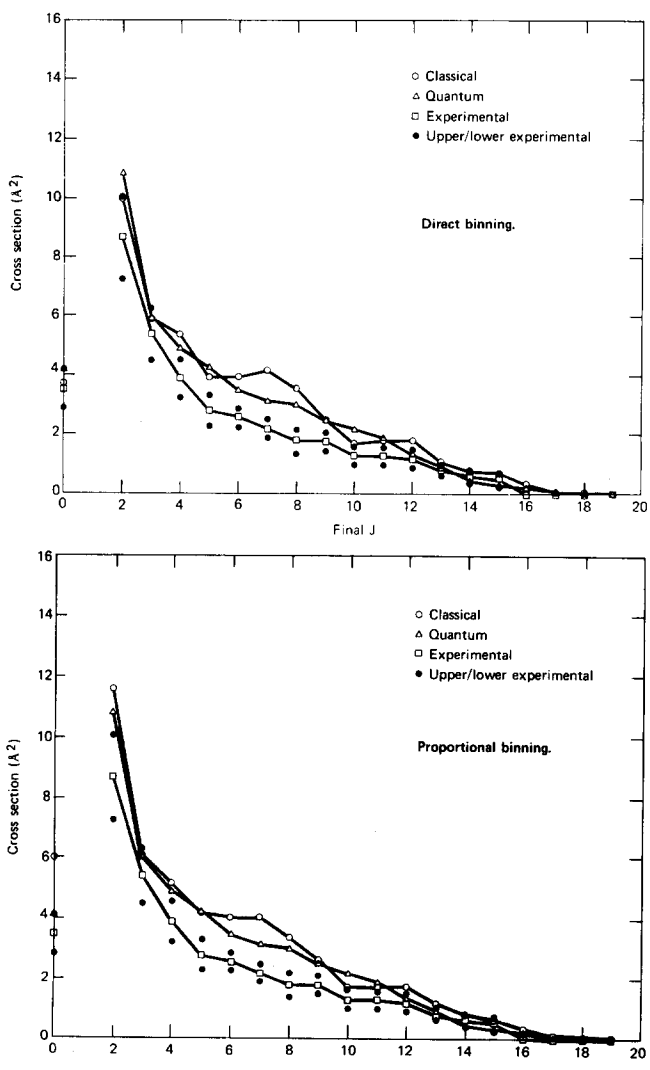

FIG. 5. Experimental and velocity averaged quantal and classical integral cross sections for rotational energy exchange as function of final rotational quantum number: (A) direct binning method, and (B) proportional binning method.

where $csm_{j'}$ represents the mathematical expectation of $f(j',b,E)$ with respect to b. This expectation is also the mathematical cross section for j'. Similarly, Eq. (10) may be recast in the following form:

$$csa_{j'} = \sum_{i=1}^{N} \phi(j',b_i,E)/N, \tag{12}$$

where $csa_{j'}$ represents the arithmetic mean of $\phi(j',b_i,E)$ with respect to b_i, and it is approximately equal to the mathematical expectation $csm_{j'}$. It is also the approximate cross section for j'. The quantity

$$\epsilon_{j'} = |csa_{j'} - csm_{j'}|$$

is the error of the Monte Carlo computation of the cross section for j'.

The distribution of $csa_{j'}$ may be approximated by a Gaussian (normal) distribution.[11] Let $s_{j'}$ be the standard deviation of $\phi(j',b_i,E)$ and α be the probability that $\epsilon_{j'}$ will be at most equal to an upper limit ϵ_α ($\epsilon_{j'} \leqslant \epsilon_\alpha$ with probability α). Then, it can be shown[4(a),11,12] that the error in the computation of $csa_{j'}$ (under the assumption of a normal distribution) is given by the following inequality:

$$\epsilon_{j'} \leqslant z_\alpha \cdot s_{j'}/\sqrt{N} \tag{13}$$

with probability (confidence level) α. The number z_α is usually found from tables of z_α vs α (see, e.g., the Appendix of Ref. 11). The values of z_α depend to a large extent on the degrees of freedom involved in the computation. However, as the number of the degrees of freedom ν increases, z_α rapidly reaches a value which changes very little with further increases of ν. Here $\nu = N - 1$, where N is the number of computed trajectories for a particular total energy E. Since N is of the order of 1000, the upper limit may be used. A confidence level of 90% ($z_\alpha = 1.645$) has been used in this paper for the estimation of $\epsilon_{j'}$. The estimate of $s_{j'}$ also involves the degrees of freedom, and it is given by

$$s_{j'} = \left[\sum_{i=1}^{N} [\phi^2(j',b_i,E) - csa_{j'}^2]/\nu\right]^{1/2}.$$

Then, from Eqs. (11) and (12), and the approximation $\nu = N - 1 \approx N$ for large N, the above equation reduces to its final form:

$$s_{j'} = 2\pi \cdot b_{\max}\left[\sum_{i=1}^{N} (b_{ij'}^2 - \bar{b}_{j'}^2)\right]^{1/2}. \tag{14}$$

The error bounds obtained by combining Eqs. (13) and (14) are given in Table II for the various cases and are shown as error bars in Figs. 3 and 4.

For the velocity-averaged cross sections, the standard deviation, denoted by $\bar{s}$, is computed from Eq. (5') which is recast here in the following form:

$$\overline{csa} = \sum_{k=1}^{3} g_k \cdot csa_k,$$

where the subscript k differentiates between the three total energies. Let $\bar{s}_{j'}$ be the standard deviation of $\overline{csa}$ and N_k be the number of trajectories (observations) at the k th total energy ($k = 1$, 2 or 3). Then assuming zero covariance, $\bar{s}_{j'}$, is given by[4(a),11-13]

TABLE III. Experimental and velocity averaged quantal and classical cross sections.

Final J	Quant. CS	Exp. CS	Exp. Err.	Direct binning Class. CS	Direct binning Class. Err.	Proportional binning Class. CS	Proportional binning Class. Err.
0	4.12	3.50	0.60	3.71	0.63	5.99	0.51
1	45.33			43.85	2.08	39.78	1.78
2	10.80	8.70	1.40	9.98	0.98	11.58	0.78
3	5.95	5.40	0.90	5.89	0.71	6.05	0.57
4	4.88	3.90	0.60	5.32	0.64	5.11	0.51
5	4.26	2.80	0.50	3.93	0.53	4.20	0.44
6	3.48	2.60	0.30	3.95	0.51	4.05	0.41
7	3.13	2.20	0.30	4.17	0.52	4.05	0.40
8	3.01	1.80	0.40	3.54	0.46	3.39	0.36
9	2.46	1.80	0.30	2.50	0.38	2.68	0.32
10	2.19	1.30	0.30	1.70	0.31	1.73	0.25
11	1.90	1.30	0.30	1.18	0.33	1.71	0.25
12	1.35	1.20	0.30	1.84	0.33	1.75	0.27
13	0.93	0.80	0.20	1.10	0.26	1.19	0.22
14	0.45	0.60	0.20	0.76	0.21	0.81	0.17
15	0.30	0.50	0.20	0.71	0.21	0.63	0.16
16	0.19	0.0	0.0	0.31	0.13	0.32	0.12
17	0.08	0.0	0.0	0.04	0.05	0.08	0.04
18	0.06	0.0	0.0	0.06	0.06	0.06	0.04
19	0.03	0.0	0.0	0.01	0.01	0.01	0.01

$$\bar{s}_{j'} = \left[\sum_{k=1}^{3} g_k \cdot s_{kj'}^2 / N_k\right]^{1/2},$$

where each $s_{kj'}$ is given by Eq. (14) evaluated at the k th total energy. The error $\bar{\epsilon}_{j'}$ of the velocity-averaged cross section for j' for a confidence level α is given by

$$\bar{\epsilon}_{j'} \leqslant z_\alpha \cdot \bar{s}_{j'}$$

with z_α obtained as before. These errors (for 90% confidence level) are given in Table III.

III. DISCUSSION

The dynamical model used in this work is that of an atom-rigid rotor. Hence there is no possibility of simulating vibrational excitation. This is reasonable in light of the experimental observations[3,14] that include only rotational energy exchange. Collisional vibrational excitation would require energies much higher than the threshold for this process.[15]

In some previous work, the classical collision mechanism between an atom and diatom has been discussed in terms of the time variation of the projection of the torque vector along a unique direction.[16] Individual trajectories for He–LiH (rigid rotor) collisions have been examined to identify characteristics of the rotational energy transfer process.[17] Again torque was found useful for understanding rotational transitions and for defining an interaction time.

The need for a realistic potential between the atom and diatom has been illustrated.[18] Using a point particle and an off-center spherical shell as a model of the He–LiH system produced cross sections for rotational energy exchange that differ drastically both in magnitude and their j' dependence from the experimental and quantal results.

In the present work, we have computed quasiclassically the rotationally inelastic integral state-to-state cross sections ($\sigma_{j-j'}$) for the LiH–He system at three different total energies using the interaction potential of paper I[1] and Figs. 1 and 2. These energies have been judiciously selected so as to closely simulate the corresponding experimental distribution.[3] For each energy, two sets of cross sections have been computed using two different methods of quantizing J (the so-called direct and proportional binning methods) and each set has been compared to the corresponding coupled states (cs) results.[2] Two sets of energy-averaged cross sections have also been computed (one for each quantization method) and they have been compared to the experimental[3] as well as to the energy averaged cs cross sections.[2]

A direct comparison between the quasiclassical and quantal results in Table II and Figs. 3 and 4 shows that for some values of j' the quantal cross sections lie outside the range of the quasiclassical error limits. First, the error limits indicated represent a 90% confidence level on the statistical averaging process. These limits would change if more trajectories were computed and if a different confidence level were chosen. Second, the quantal calculations incorporate certain inherent approximations whose effects are not indicated by "error" bars. If it were possible to place such limits on the quantal calculations, then there might be complete overlap between the ranges of the quantal and quasiclassical error limits. For these reasons it is not clear whether or not the small differences between the calculations are significant.

A noticeable feature of both the quasiclassical and quantal cross sections in Figs. 3 and 4 is the undulatory behavior rather than a monotonic decrease as a function of j'. This structure is reminiscent of the "rotational rainbow" structure in differential rotationally inelastic cross sections first described in classical trajectory studies of Li^+–CO collisions.[19] Some experimental evidence for rotational rainbows in differential cross sections has been reported.[20] It has been also seen in earlier calculations of integral rotationally inelastic cross sections for other atom–molecule systems.[21] Here in Fig. 5, it is interesting to observe that the undulations are strongly damped in the energy-averaged quantal calculation, but much less well damped by the energy averaging in the quasiclassical case. Therefore the structure re-

mains prominent in the quasiclassical cross sections in Fig. 5.

The energy-averaged quasiclassical cross sections compare very well to the corresponding quantal results, even better than the agreement between the single energy results. This is probably due to the averaging process which has brought three times as many trajectories into the energy-averaged calculation. The agreement between the quasiclassical energy-averaged and experimental cross sections is about as good as that between the cs energy averaged and experimental cross sections. Thus, we conclude that for the present system the quasiclassical method proves to be an acceptable approximation for the computation of integral cross sections.

[1]D. M. Silver, J. Chem. Phys. **72**, 6445 (1980).
[2]E. F. Jendrek and M. H. Alexander, J. Chem. Phys. **72**, 6452 (1980).
[3]P. J. Dagdigian and B. E. Wilcomb, J. Chem. Phys. **72**, 6462 (1980).
[4]*The Monte Carlo Method*, edited by Yu. A. Shreider (Pergamon, New York, 1966); J. M. Hammersley and D. C. Handscomb, *Monte Carlo Methods* (Wiley, New York, 1964); J. H. Halton, SIAM Rev. **12**, 1 (1970); S. Haber, *ibid.* **12**, 481 (1970).
[5]R. A. La Budde and R. B. Bernstein, J. Chem. Phys. **55**, 5499 (1971).
[6]S. Chapman and S. Green, J. Chem. Phys. **67**, 2317 (1977).
[7]M. Karplus, R. N. Porter, and R. D. Sharma, J. Chem. Phys. **43**, 3259 (1965).
[8]H. Goldstein, *Classical Mechanics* (Addison–Wesley, Reading, MA, 1965).
[9]F. Ceschino and J. Kuntzmann, *Numerical Solution of Initial Value Problems* (Prentice–Hall, Englewood Cliffs, NJ, 1966); Ralston and Wilf, *Mathematical Methods for Digital Computers* (Wiley, New York, 1960).
[10]E. F. Pearson and W. Gordy, Phys. Rev. **177**, 59 (1969).
[11]K. A. Brownlee, *Statistical Theory and Methodology in Science and Engineering* (Wiley, New York, 1965).
[12]Notice that $csa_{j\cdot}$ itself is an average of N observations. If $s_{j\cdot}$ is the standard deviation of these observations, then the quantity $s_{j\cdot}/\sqrt{N}$ represents the standard deviation of their average (namely $csa_{j\cdot}$), assuming normal distribution.
[13]If σ_i^2 is the variance of a random variable x_i, and if a_i are numerical coefficients, then the variance of the random variable $x = \Sigma_i\, a_i x_i$ is given by the equation $\sigma_x^2 = \Sigma_i\, a_i^2 \cdot \sigma_i^2 + \frac{1}{2}\Sigma_{i,j}\, a_i a_j \sigma_{ij}\delta_{ij}$ are the covariances of the random numbers x_i and x_j.
[14]O. Nédélec and J. Dufayard, J. Chem. Phys. **76**, 378 (1982).
[15]P. J. Dagdigian, Chem. Phys. **52**, 279 (1980).
[16]A. Metropoulos, Chem. Phys. Lett. **89**, 405 (1982).
[17]A. Metropoulos and D. M. Silver, Chem. Phys. Lett. **93**, 247 (1982).
[18]M. H. Alexander and P. J. Dagdigian, J. Chem. Phys. **73**, 1233 (1980).
[19]L. D. Thomas, J. Chem. Phys. **67**, 5224 (1977).
[20]R. Schinke and P. McGuire, Chem. Phys. **28**, 129 (1978).
[21]W. Eastes, U. Ross, and J. P. Toennies, Chem. Phys. **39**, 407 (1979); W. Schepper, U. Ross, and D. Beck, Z. Phys. A **290**, 131 (1979); K. Bergmann, R. Englehardt, U. Hefter, and J. Witt, J. Chem. Phys. **71**, 2726 (1979).